NASA Technical Memorandum 79274

STREAKLINE FLOW VISUALIZATION STUDY OF A HORSESHOE VORTEX IN A LARGE-SCALE, TWO-DIMENSIONAL TURBINE STATOR CASCADE

Raymond E. Gaugler and Louis M. Russell
Lewis Research Center
Cleveland, Ohio

Prepared for the
Twenty-fifth International Gas Turbine Conference and Products Show
sponsored by the American Society of Mechanical Engineers
New Orleans, Louisiana, March 9-13, 1980

STREAKLINE FLOW VISUALIZATION STUDY OF A HORSESHOE VORTEX IN A LARGE-SCALE, TWO-DIMENSIONAL TURBINE STATOR CASCADE

Raymond E. Gaugler and Louis M. Russell

National Aeronautics and Space Administration
Lewis Research Center
Cleveland, Ohio

INTRODUCTION

The heat transfer to the components of a gas turbine is influenced by the various flow mechanisms encountered, as described in the survey paper by Graham (1). One of the mechanisms, secondary flow, has been shown to have a very pronounced effect, especially on the endwall surfaces near the intersections with the vanes. Blair (2), and Graziani, et al (3) measured the heat transfer from the endwall in a large scale, two-dimensional turbine rotor cascade, and presented Stanton number contour plots. They concluded that the secondary flows greatly influenced the heat transfer on the cascade endwall and on the vane suction surface. They observed especially steep gradients in heat transfer on the endwall in the vicinity of the vane leading edge. As shown by Langston, et al. (4), it is in this region that the incoming endwall boundary-layer rolls up into a horseshoe vortex that wraps around the leading edge. One leg of this vortex stays close to the suction side corner as it is swept downstream, while the pressure side leg is driven across the passage by the pressure difference, as it moves downstream, becoming part of the passage vortex. Graziani, et al. (3) showed the extent of the influence of this vortex system on their heat transfer results by presenting pictures of ink traces of limiting streamlines on the endwall of their cascade.

Aerodynamic investigations of the secondary flow patterns have been the object of flow visualization studies for some time. Using smoke, Herzig, et al. (5) observed the roll-up of the endwall boundary layer into a passage vortex, but they did not observe the vortex in the vicinity of the leading edge. They showed very clearly that the deflection of the boundary layer flow from pressure side to suction side varies strongly with distance from the endwall, with the fluid nearer the wall being affected the most. Langston, et al. (4), made detailed aerodynamic measurements in a large scale turbine rotor cascade, including endwall flow visualization and smoke addition to the boundary-layer. They observed the limiting streamlines on the endwall associated with the leading edge horseshoe vortex, and noted that all of the smoke introduced into the endwall inlet boundary-layer ended up in the passage vortex. Marchal and Sieverding (6) used smoke and a laser light sheet to visualize a cross section of the flow near the leading edge for both a turbine rotor cascade and a turbine stator cascade. With this technique, they obtained a view of the flow pattern in a plane at an instant in time, but do not show the spatial development of the vortex.

Thus it was decided to conduct an experimental study of the endwall-leading edge region to show more detail of the roll-up of the boundary layer and development of a horseshoe vortex, and the relation of the vortex to the flow traces observed on passage endwalls. In addition, this work provides a background against which efforts can be directed to modify or control the local effects of the leading edge vortex.

In the present study, the horseshoe vortex was visualized by injecting neutrally bouyant, helium filled bubbles into the boundary layer upstream of the leading edge of a two-dimensional turbine stator cascade, and recording the bubble paths as streaks on photographic film. Since the bubbles follow streamlines without diffusing as smoke does, the streaklines observed represent the complete time history of inidividual fluid particles. Therefore, details of the horseshoe vortex structure were seen that have never been reported before. Also, endwall flow traces were observed, using a mixture of oil and a yellow pigment.

The cascade contained six vanes, with a profile that was scaled up three times from that used in the NASA Lewis High Pressure Turbine Facility (7). Air

flow through the cascade was drawn in from an atmospheric inlet and exhausted to the laboratory altitude exhaust system. Inlet Reynolds number, based on true chord, ranged between 1.0×10^5 to 3.0×10^5 for the tests described. Bubble paths were recorded photographically using both a motion picture camera and a 35 mm still camera.

APPARATUS AND PROCEDURE

The vanes used in the cascade were fabricated to the surface coordinates shown in Fig. 1. These coordinate values are three times the mean section values of the turbine vanes designed for use in the NASA Lewis High Pressure Turbine Facility (7). However, the span of the vanes in the test cascade was four times the actual vanes, due to a requirement to match the cascade with existing hardware. This change in aspect ratio should not affect the results of the tests, since the phenomenon under study is concentrated in the vicinity of the passage endwall. The pertinent cascade parameters were: axial chord, 11.4 cm (4.48 in.); chord/axial chord, 1.46; pitch/axial chord, 1.08; aspect ratio (span/axial chord), 1.34; air inlet angle, 0° (axial); air exit angle, 67°.

The wind tunnel built to hold the cascade is shown schematically in Fig. 2(a). The inlet was designed for constant acceleration of the flow through it, as described in Ref. 8. At the end of the inlet section the flow enters a duct, 68.6 cm (27 in.) wide by 15.2 cm (6 in.) high by 152.4 cm (60 in.) long. The cascade of six vanes is located at the end of this section. Vane pitch is 12.3 cm (4.84 in.), three times actual size. The end vanes have adjustable tailboards to assure periodicity of the flow through the cascade. From the cascade, the flow is ducted to the laboratory altitude exhaust system. Figure 2(b) is a photograph of the cascade test section. The vanes were fabricated from wood and painted black. The rest of the cascade was built from clear acrylic plastic, with the bottom endwall painted black.

There is a slot in the endwall located about 21 cm (8.25 in.) upstream of the vane leading edges. The helium bubbles used for flow visualization are injected into the boundary layer from a plenum beneath this slot. The bubble generating system is described in detail by Hale, et al. (9) and an example of its use for visualization of film cooling was presented by Colladay and Russell (10). Figure 3 shows a cross section of the bubble generator head. The bubble solution flows through the annular passage and is formed into a bubble inflated with the helium passing through the inner concentric tube. The bubble is blown off the tip by a continuous blast of air flowing through the shroud passage. The desired bubble size and neutral bouyancy are achieved by proper adjustment of air, bubble solution, and helium flow rates. As many as 300 bubbles per second are formed in this device. For these tests the bubble diameter was about 1.5 mm (0.06 in.). The bubble generator head was placed through a grommet in the wall of the plenum beneath the injection slot. The actual rate of bubble injection into the cascade boundary layer was about 13 per second, based on a number of one second time exposures of the flow. The reduced rate resulted from bubbles in the plenum colliding with the walls and bursting before reaching the injection slot.

The light source for bubble illumination consisted of a 300 watt quartz arc lamp, a rectangular aperture, and a 300 mm lens. The light source was located upstream of the tunnel inlet nozzle and projected a beam down the tunnel into the cascade. The image of the aperture was focused in the cascade, just off the endwall surface. When viewed from above, or from the side, the bubbles showed up very brightly when they were in the light beam. Photographs of the bubbles were taken from two locations, directly above the cascade, providing a plan view of the flow, and upstream of the cascade, looking through the tunnel sidewall into the cascade, providing a perspective view of the flow. At both locations, a motion picture camera, running at either 3 or 12 frames per second, was used to record the bubble traces. Also, for the plan view, a series of one second time exposures were taken with a 35 mm still camera. The movies that were taken have to be considered as a collection of independent data records, since the time of flight of the bubbles through the field of view was much shorter than the open time of the shutter. Thus, the bubbles appear as streaklines on the film, and adjacent frames of the film can never show the same bubble. The combination of low bubble injection rate and camera shutter speed resulted in only about one film frame in every one hundred containing something of interest. The procedure was to view the movie film, one frame at a time, and make a 35 mm negative of the interesting frames.

In addition to photographing bubble traces, drops of oil, mixed with a yellow pigment, were placed on the endwall and allowed to flow when the tunnel was run. The smeared-out drops were then photographed, presenting a view of limiting streamlines on the surface.

The cascade was run over a range of inlet Reynolds number, based on true chord, of 1.3×10^5 to 3.0×10^5, corresponding to a tunnel inlet velocity range of about 12.5 m/sec (41.0 ft/sec) to 28.6 m/sec (94.0 ft/sec). Over this range of velocity, there was no change observed in the behavior of the horseshoe vortex, so it was decided to run at the lower velocity for all data pictures, since the slower bubbles were easier to photograph. Periodicity of the cascade was set by monitoring the endwall static pressures in the center of each passage at the cascade exit and adjusting the tailboards. Figure 4 shows the pressures measured, for two different velocity levels, after final setting of the tailboards. The pressures are referenced to atmospheric.

The tunnel boundary layer profile was measured at a point 21.6 cm (8.5 in.) upstream of the vanes.

RESULTS AND DISCUSSION

All the results presented herein are for the tunnel running with a free-stream velocity of about 13.1 m/sec (43.0 ft/sec) unless otherwise specified. As noted in the preceding section, the lower tunnel velocity gave brighter bubble traces on the film.

The velocity profile through the endwall boundary layer was surveyed with a total pressure probe at a point 1.4 passage heights upstream of the vanes. The dimensionless profile is shown in Fig. 5. Also included in Fig. 5 is the logarithmic distribution in the wall region for a fully turbulent boundary layer, from Schlichting (11). The boundary layer thickness, defined as the point where the velocity is 99 percent of the free-stream value, was 1.81 cm (0.714 in.). Momentum thickness was 0.165 cm (0.065 in.) and the boundary layer shape factor was 1.27. Momentum thickness Reynolds number was 1389. These values are as would be expected for an equilibrium turbulent boundary layer.

The limiting streamlines on the endwall surface, as evidenced by oil traces, are discussed first. Figure 6 is a representative photograph of the oil drop traces observed in these tests, with the location of the three-dimensional separation saddle point indicated. Due to the fact that this cascade had a smaller turning, and thus a milder pressure gradient across the passage, the saddle point is much closer to the vane than shown for the blades in Ref. 4. The three-dimensional separation line that crosses the passage from the saddle point to the suction side of the adjacent vane reaches that vane surface at about 50 percent of axial chord. At that location, the oil streaks were observed visually to flow up the suction surface and curve back toward the trailing edge. Near the cascade exit, the endwall oil streaks were seen to flow directly across the passage in a tangential direction, from the pressure side to the suction side. The endwall oil traces in the wake region behind the vane trailing edge region followed the vane exit angle smoothly, further indicating good periodicity for the cascade. Comparison of the endwall flow traces of this work with that of Marchal and Sieverding (6), who used a vane of similar profile, shows good agreement.

The endwall traces just discussed provide a visible boundary condition on the three-dimensional secondary flows. At the other extreme, outside the boundary layer, the potential flow solution provides the limit. In between these two regions, in the boundary layer, is where the bubble traces are followed.

Figure 7 shows representative pictures of the overhead view of bubble streaklines through the cascade. These views were extracted from the 16 mm movies made of the tests. The height of the light beam was about 7.6 cm (3 in.) in this test, considerably higher than the boundary layer thickness, so bubbles that have reached the free stream will still be visible in some photographs. The bright spots on the endwall in these photographs are reflections from the residue of bubbles that have burst in the passage. Figure 7(a) is a schematic of the camera field of view, showing the orientation of the flow and light beam. Figure 7(b) shows the traces of some bubbles that are out of the boundary layer, and unaffected by the secondary flows. Figure 7(c) shows two streaklines, one apparently out of the boundary layer, following a potential flow streamline, and one in the outer portion of the boundary layer that has been entrained into the horseshoe vortex. Figure 7(d) shows a strealine for a bubble close to the wall that has been trapped in the vortex core. The twists in the streakline indicate that bubble is in a region of flow with intense rotation. From Fig. 8, some further insight into the vortex form can be gathered. In these oblique views, looking downstream, the three dimensional nature of the flow is dramatically evident. For these tests, the light beam extended from the endwall surface to about 0.9 cm (0.37 in.) above it, assuring that all bubbles seen were in the boundary layer. Figure 8(a) is a view into the cascade with the room lights on, included here for orientation purposes. In Fig. 8(b), a bubble streakline follows a tight corkscrew path as it follows the core of the horseshoe vortex. In Fig. 8(c) a bubble appears to follow a more relaxed twisting path, such as would be expected for fluid particles further from the vortex core. In Figs. 8(b) and (c), note that reflections of the bubble streaks can be seen on the endwall surface. The distance between the streakline and its reflection is a measure of distance from the wall. In Fig. 8(b) the bubble appears to be entering the cascade much closer to the wall than in Fig. 8(c). Thus the bubble in Fig. 8(b) is in the inner region of the boundary layer, where the vorticity is higher, and ends up forming the core of the horseshoe vortex.

Figure 9 is another plan view of the cascade, with the streaklines of bubbles in the horseshoe vortex traced from a number of 16 mm movie frames. When this movie was made, the light source was located at the side of the tunnel, projecting a beam through the sidewall. This provided illumination further into the cascade than when the light was directly upstream. With this arrangement, the bubbles were illuminated all the way to the trailing edge plane of the cascade. The most striking feature in Fig. 9 is that the core of the vortex remains in the middle of the passage, all the way to the exit plane.

Figure 10 is a composite tracing showing the oil traces on the endwall and the limit of the vortex path taken from Fig. 9. Note that near the leading edge, the vortex path is closely following the endwall limiting streamlines, but further down the passage there is a big difference in direction between the two. This is the same type of behavior as noted by Marchal and Sieverding (6) for their stator cascade. The fact that the vortex location in the stator cascade is markedly different than observed in a rotor cascade implies that the heat transfer patterns on the endwall will also be different. There is some additional evidence of this seen when the work of Georgiou, et al. (12) is compared with that of Graziani, et al. (3). Georgiou, et al. (12) reported iso-heat transfer lines for a stator cascade similar to the one used by Marchal and Sieverding (6). In their work, the location of the maximum endwall heat flux near the cascade exit appears to be near the middle of the passage, whereas in Graziani, et al. (3) it appears to be closer to the suction surface.

CONCLUDING REMARKS

Streakline flow visualization using neutrally bouyant bubbles has been used in conjunction with endwall oil flow traces to show details of the development of the horseshoe vortex and subsequent passage vortex in a two-dimensional turbine stator cascade. Plan view pictures of the bubble streaklines and oblique, perspective views show that the fluid closest to the wall in the inlet boundary layer rolls up to form a tight vortex core. Fluid from further out in the boundary layer is entrained in this vortex. Comparison of the bubble streaklines with oil flow traces on the endwall show that the path of the vortex is aligned more with the free-stream flow than with the endwall limiting streamlines. Near the trailing edge, the vortex core was observed to be about midway between the pressure and suction sides of the passage.

REFERENCES

1 Graham, R. W., "Fundamental Mechanisms that Influence the Estimate of Heat Transfer to Gas Turbine Blades," ASME Paper No. 79-HT-43, Aug. 1979.

2 Blair, M. F., "An Experimental Study of Heat Transfer and Film Cooling on Large-Scale Turbine Endwalls," ASME Journal of Heat Transfer, Vol. 96, No. 4, Nov. 1974, pp. 524-529.

3 Graziani, R. A., Blair, M. F., Taylor, J. R., and Mayle, R. E., "An Experimental Study of Endwall and Airfoil Surface Heat Transfer in a Large Scale Turbine Blade Cascade," ASME Paper No. 79-GT-99, Mar. 1979.

4 Langston, L. S., Nice, M. L., and Hooper, R. M., "Three-Dimensional Flow Within a Turbine Cascade Passage," ASME Journal of Engineering for Power, Vol. 99, No. 1, Jan. 1977, pp. 21-28.

5 Herzig, H. Z., Hansen, A. G., and Costello, G. R., "A Visualization Study of Secondary Flows in Cascades," NACA Report 1163, 1954.

6 Marchal, Ph. and Sieverding, C. H., "Secondary Flows Within Turbomachinery Bladings," Secondary Flows in Turbomachines, AGARD-CP-214, Advisory Group for Aerospace Research and Development, Paris (France), 1977, Paper 11.

7 Szanca, E. M., Schum, H. J., and Hotz, G. M., "Research Turbine for High-Temperature Core Engine Application. I: Cold-Air Overall Performance of Solid Scaled Turbine," NASA TN D-7557, 1974.

8 Yuska, J. A., Diedrich, J. H., and Clough, N., "Lewis 9- by 15-Foot V/STOL Wind Tunnel," NASA TM X-2305, 1971.

9 Hale, R. W., Tan, P., Stowell, R. C., and Ordway, D. E., "Development of an Integrated System for Flow Visualization in Air Using Neutrally-Bouyant Bubbles," SAI-RR 7107, Sage Action, Inc., Ithaca, N.Y., Dec. 1971. (AD-756691)

10 Colladay, R. S. and Russell, L. M., "Streakline Flow Visualization of Discrete-Hole Film Cooling with Normal, Slanted, and Compound Angle Injection," NASA TN D-8248, 1976.

11 Schlichting, H., "Boundary Layer Theory," 6th Edition, Mcgraw-Hill, New York, 1968.

12 Georgiou, D. P., Godard, M., and Richards, B. E., "Experimental Study of the Iso-Heat-Transfer-Rate Lines on the End-Wall of a Turbine Cascade," ASME Paper No. 79-GT-20, , 1979.

X		Y_L		Y_U	
cm	in.	cm	in.	cm	in.
0.000	0.000	1.524	0.600	1.524	0.600
.305	.120	.610	.240	2.438	.960
.381	.150	.518	.204	2.553	1.005
.762	.300	.206	.081	3.018	1.188
1.143	0.450	0.046	0.018	3.368	1.326
1.524	.600	.0	.0	3.642	1.434
1.905	.750	.046	.018	3.863	1.521
2.286	.900	.191	.075	4.039	1.590
2.667	1.050	0.358	0.141	4.176	1.644
3.048	1.200	.495	.195	4.282	1.686
3.429	1.350	.617	.243	4.359	1.716
3.810	1.500	.724	.285	4.404	1.734
4.191	1.650	0.800	0.315	4.420	1.740
4.572	1.800	.876	.345	4.427	1.743
5.334	2.100	.991	.390	4.389	1.728
6.858	2.700	1.118	.440	4.145	1.632
8.382	3.300	1.143	0.450	3.772	1.485
9.906	3.900	1.059	.417	3.330	1.311
11.430	4.500	.891	.351	2.835	1.116
12.954	5.100	.663	.261	2.240	.882
14.478	5.700	0.396	0.156	1.554	0.612
16.002	6.300	.076	.030	.777	.306
16.657	6.558	.267	.105	.267	.105

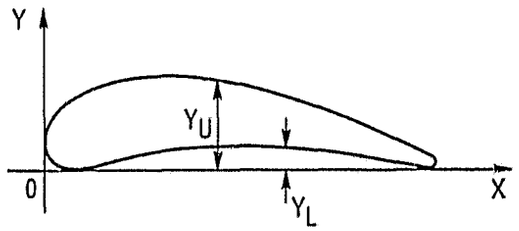

Figure 1. - Vane coordinates.

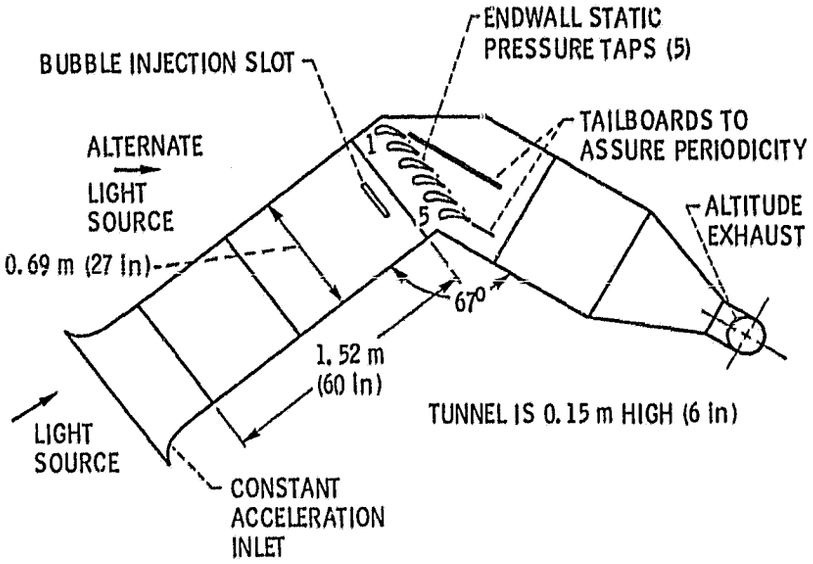

(a) SCHEMATIC PLAN VIEW.

Figure 2. - Flow visualization rig.

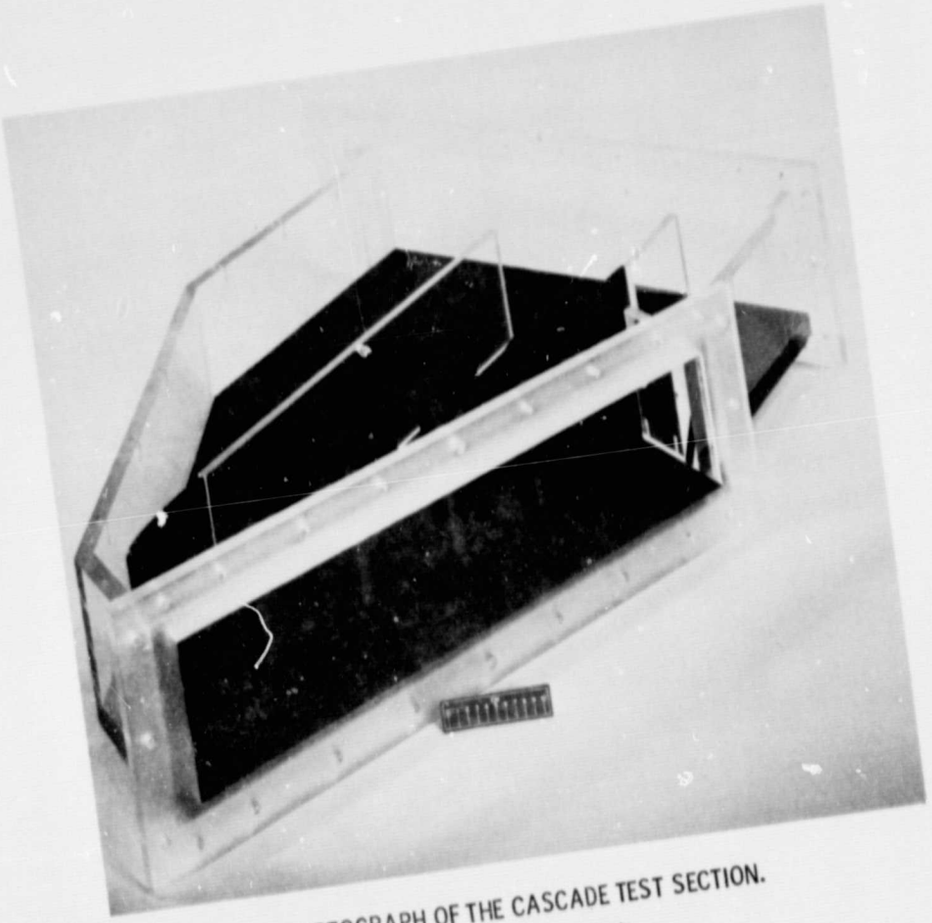

(b) PHOTOGRAPH OF THE CASCADE TEST SECTION.

Figure 2. - Concluded.

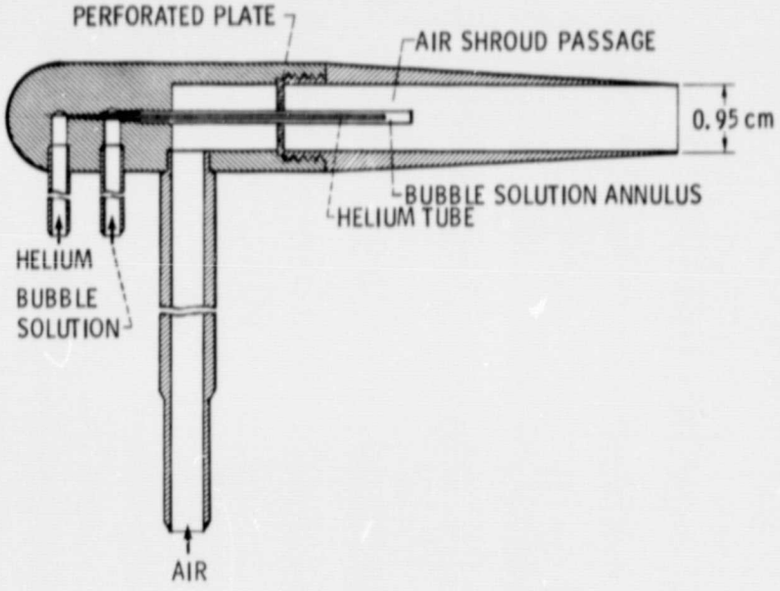

Figure 3. - Bubble generator head.

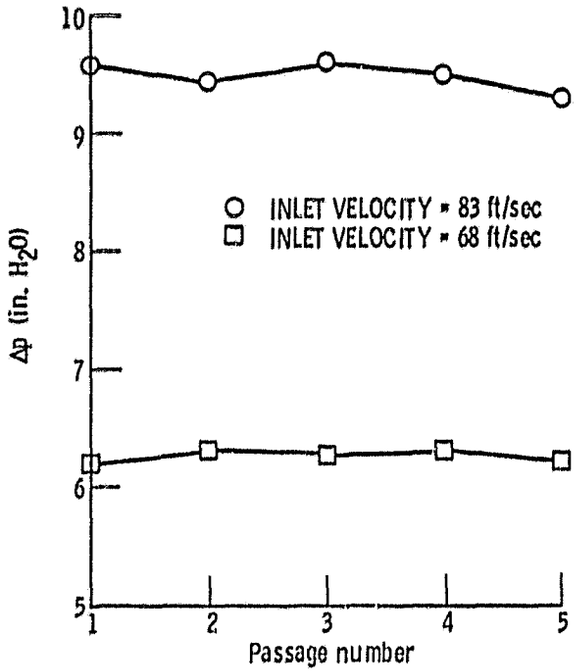

Figure 4. - Cascade periodicity.

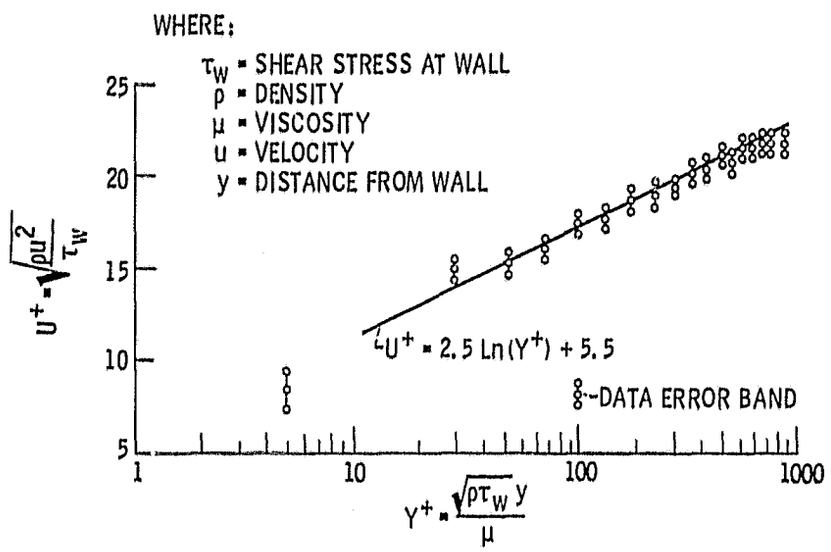

Figure 5. - Boundary layer profile at entrance to vanes.

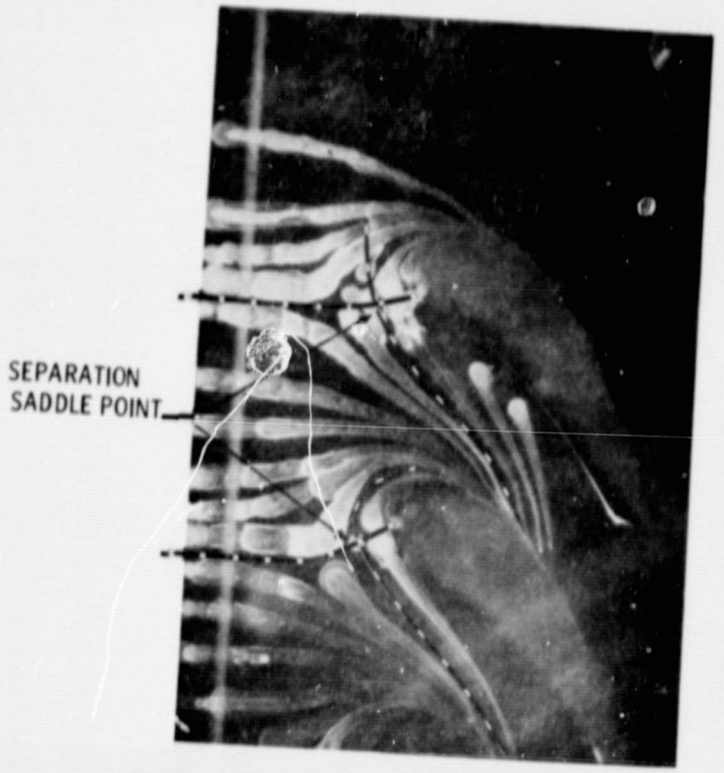

Figure 6. - Photograph of endwall oil traces.

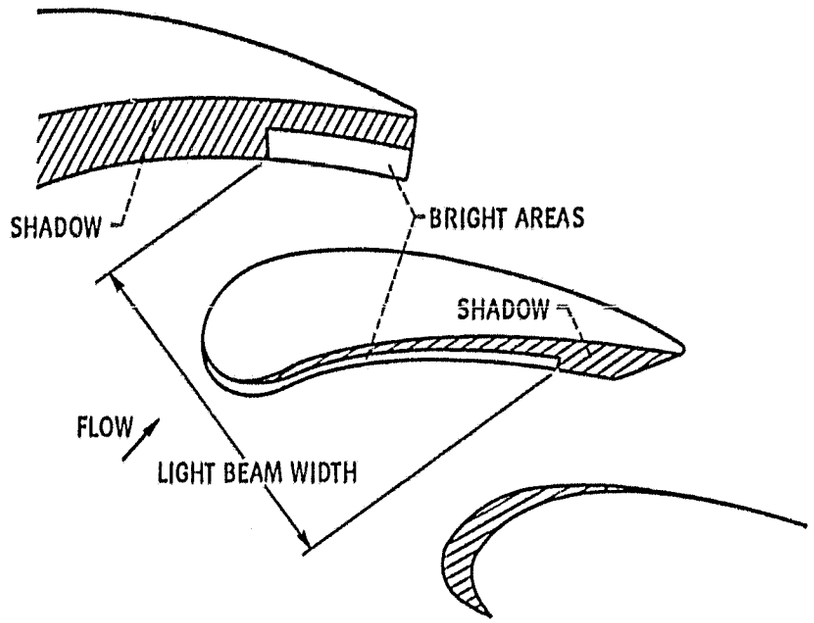

(a) SCHEMATIC OF THE VIEW SHOWN IN PHOTOGRAPHS.

Figure 7. - Photographs of bubble streaklines.

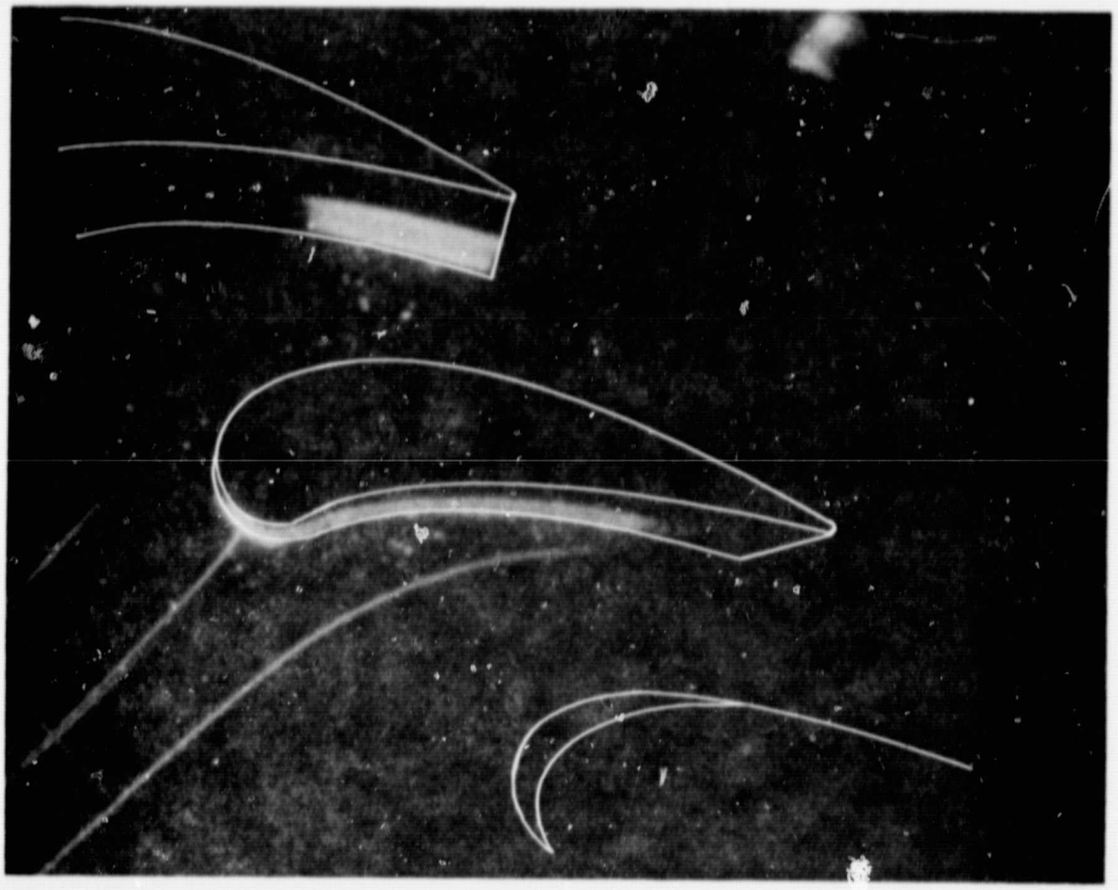

(b) BUBBLES IN THE FREE STREAM

Figure 7. - Continued.

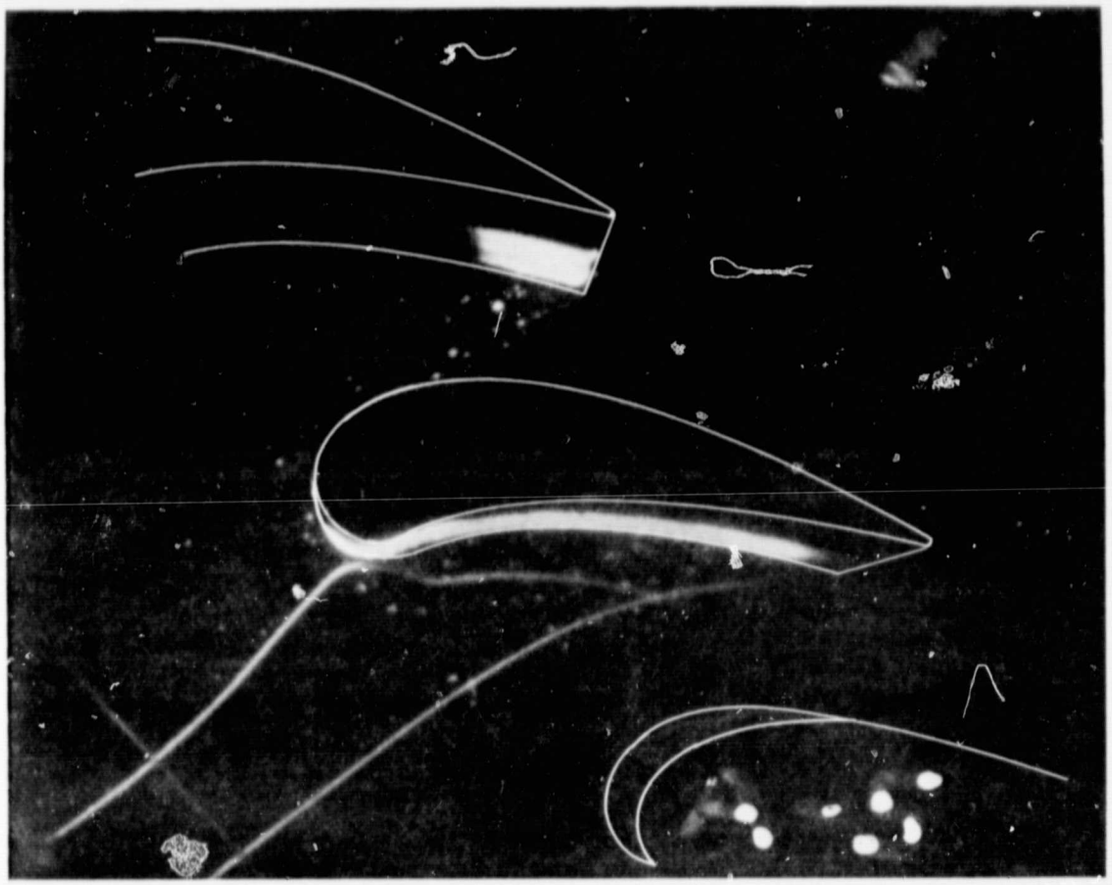

(c) BUBBLE IN OUTER REGION OF VORTEX AND A BUBBLE IN FREE STREAM.

Figure 7. - Continued.

(d) BUBBLE IN HORSESHOE VORTEX CORE.

Figure 7. - Concluded.

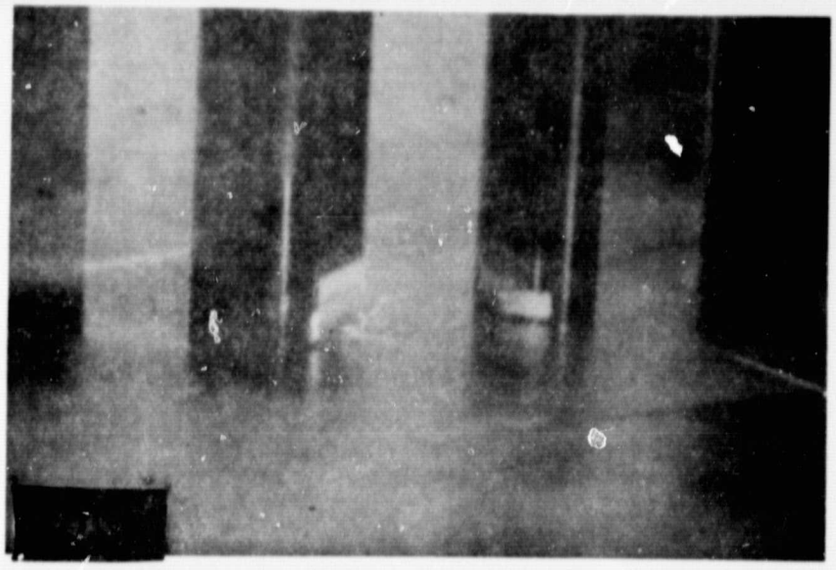

(a) FULLY LIGHTED VIEW OF THE CASCADE INLET.

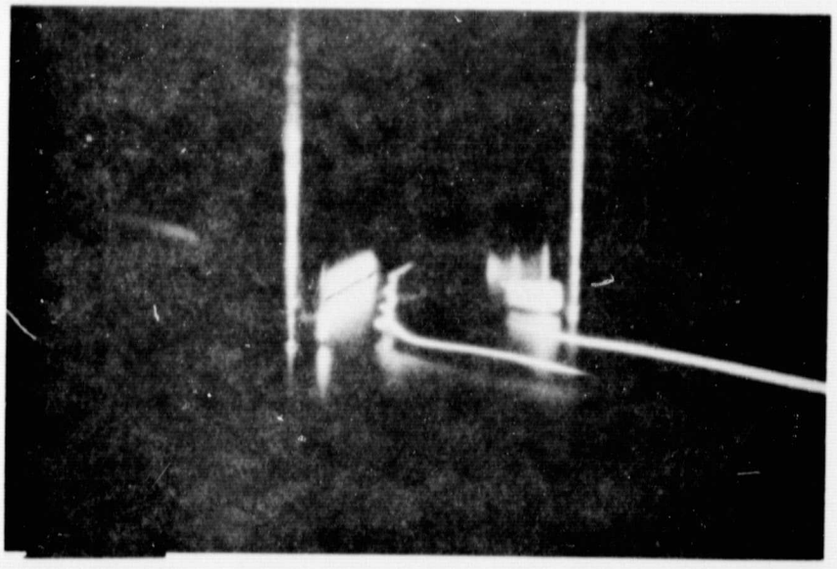

(b) BUBBLE IN VORTEX CORE.

Figure 8. - Oblique view of pressure side leg of horseshoe vortex.

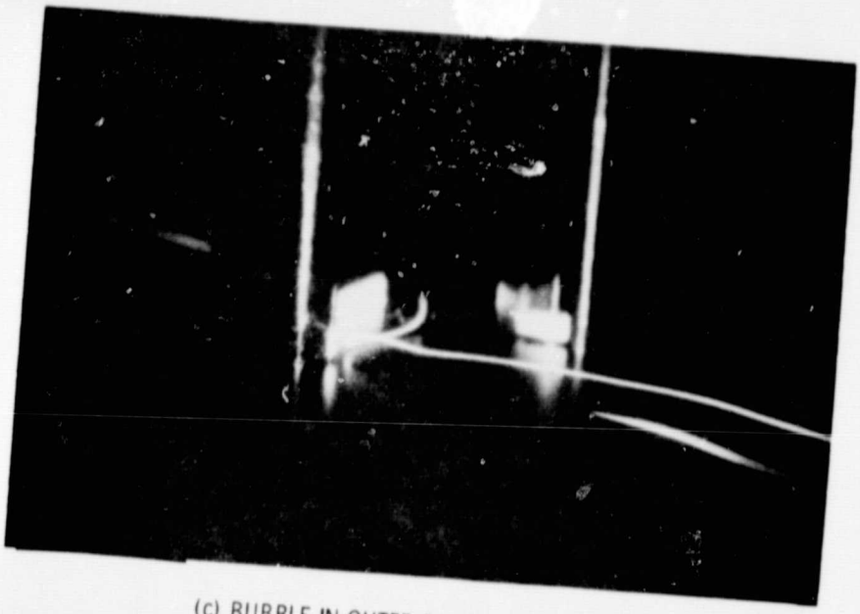

(c) BUBBLE IN OUTER REGION OF VORTEX.

Figure 8. - Concluded

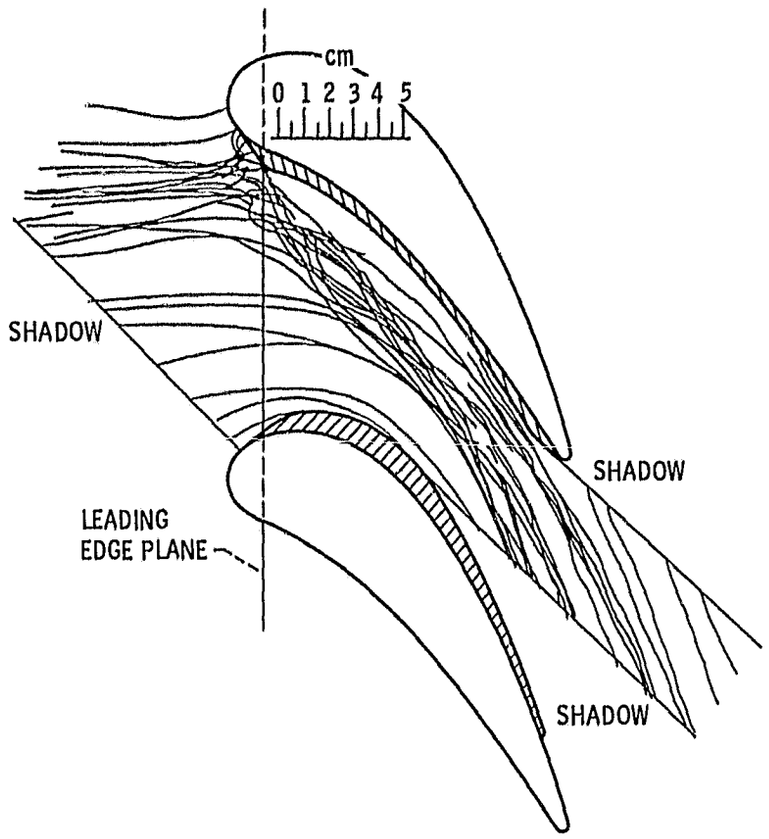

Figure 9. - Composite of bubble streaklines from 16 mm movie frames.

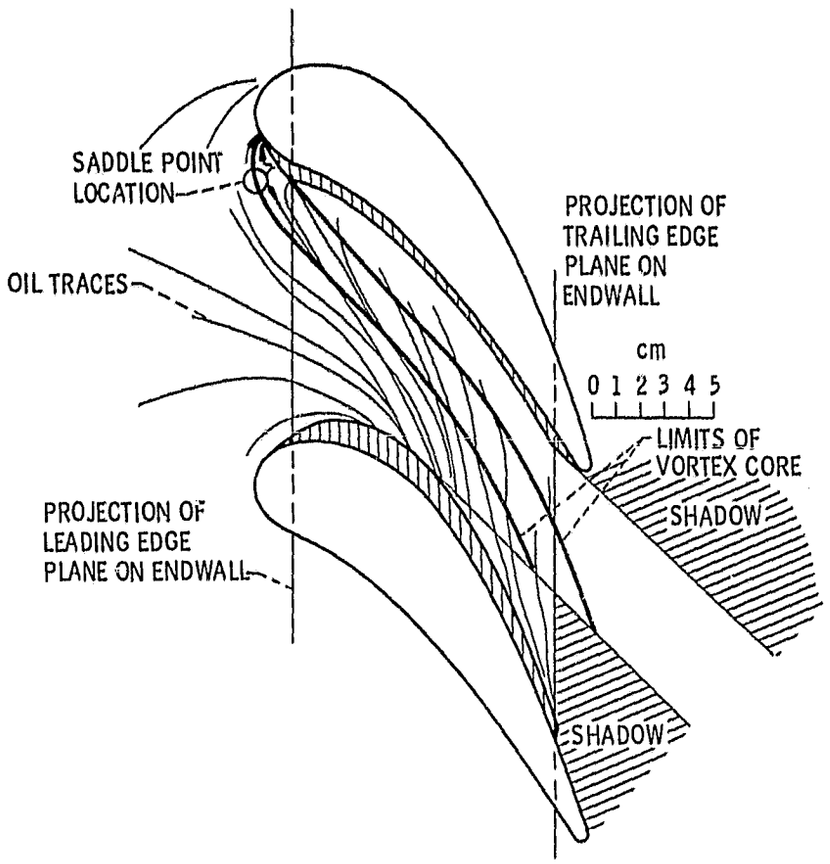

Figure 10. - Location of vortex superimposed on endwall oil traces.